Mechanical Testing of Connections Blind Bolted to the Thick Glass-Fiber-Reinforced Polymer Spar Cap of a Decommissioned GE37 Wind Turbine Blade

Ammar A. Alshannaq, A.M.ASCE[1]; John A. Respert[2]; Lawrence C. Bank, Dist.M.ASCE[3]; David W. Scott, M.ASCE[4]; and T. Russell Gentry[5]

Abstract: Millions of tons of glass-fiber-reinforced polymer (GFRP) composite wind turbine blades are expected to age out of service over the next 30 years. Research is being conducted on repurposing these structures as new civil infrastructure products. The GFRP material in these decommissioned wind blades has been shown to retain significant strength and stiffness for second-life applications. However, for repurposing as new products, they will need to be connected to other structural members. The connections employed for this need to be designed, evaluated, and tested prior to their use. Here, we present the results of detailed testing of bolted connections for load-carrying appurtenances that will carry the phases and shield wires (e.g., insulators, crossarms, davits, guy wires, posts) to the spar cap of an 11-year-old 1.5 MW GE37 wind blade, intended for use as a repurposed transmission pole (i.e., a BladePole). Details of ASTM-type pull-out and bearing capacity tests using different types of blind bolts, and tests of a full-scale steel bracket connection called a "universal connector," are reported. The effects of the different blind bolts, pin diameters, and loading directions relative to the composite laminate structure (longitudinal or transverse) for both the coupon- and full-scale connector bracket tests are described. The ability to design and construct robust connections for repurposed wind blade structures was demonstrated. **DOI: 10.1061/JCCOF2.CCENG-4101**.

Author keywords: Fiber-reinforced polymer; Structural repurposing; Second-life applications; Decommissioned wind blades; Pull-out testing; Pin-bearing testing; Full-scale testing.

Introduction

Fiber-reinforced polymer (FRP) composites have become popular over the last few decades in the civil engineering industry and in research studies due to their high strength-to-weight ratios, high stiffness-to-weight ratios, reduced weight relative to other structural materials, corrosion resistance, fatigue resistance, and durability (Bank 2006). One of the major structural applications of glass FRP (GFRP) composite materials is in wind turbine blades, in which relatively thick laminates are attached to lightweight sandwich airfoil shells, providing highly complex geometries, lightweight structures, and substantial fatigue resistance. The typical wind turbine is characterized by three long cantilevering blades that rotate around a hub, generating electricity. However, these structures often have a design life of only 20–25 years due to the uncertainty associated with fatigue loading during their service (Brøndsted et al. 2005; Mishnaevsky et al. 2017). In fact, they may have a service life of even less than 20 years due to obsolescence in the rapidly expanding wind industry (Bank et al. 2021). Consequently, when they are removed from the turbine, they retain significant structural capacity.

With wind turbine production increasing rapidly, there is a threat to the environment from the millions of tons of nonbiodegradable FRP composites expected to be decommissioned over the next 30 years (Liu and Barlow 2017; Cooperman et al. 2021). The disposal of GFRP materials involves landfilling and/or incineration, mechanical grinding, or thermal/chemical processing. Some of these processes are environmentally harmful (i.e., landfilling or incineration), while the others (i.e., mechanical or thermal/chemical) are not economically viable, making them less attractive (Oliveux et al. 2015; Jensen and Skelton 2018; Chen et al. 2019). Added to this, the relatively short service lives of these structures in their first incarnations as wind blades presents an option for their viable structural repurposing. The structural repurposing of these composites is attracting attention from researchers, with full-sized decommissioned wind turbine blades or large cut parts having the potential for use as load-bearing elements in new civil infrastructure, which typically involves large structures at relatively low stresses being used in harsh environments where durability is often the main concern (Goodman 2010; Joustra et al. 2021a, b; McDonald et al. 2022). Details of a design for using wind blades as girders in a pedestrian bridge have been described in Suhail et al. (2019) and such a bridge has been

[1]Assistant Professor, Dept. of Civil Engineering, Yarmouk Univ., P. O. Box 566, Irbid 21163, Jordan (corresponding author). ORCID: https://orcid.org/0000-0002-3455-3784. Email: aalshannaq@yu.edu.jo

[2]Undergraduate Student, School of Mechanical Engineering, Georgia Institute of Technology, 801 Ferst Dr., Atlanta, GA 30332. Email: jrespert3@gatech.edu

[3]Research Faculty, School of Architecture, Georgia Institute of Technology, 245 4th St NW, Atlanta, GA 30332. ORCID: https://orcid.org/0000-0002-4279-4473. Email: lbank3@gatech.edu

[4]Professor and Chair, Dept. of Civil Engineering and Construction, Georgia Southern Univ., P. O. Box 8077, Statesboro, GA 30460. Email: dscott@georgiasouthern.edu

[5]Professor, School of Architecture, Georgia Institute of Technology, 245 4th St NW, Atlanta, GA 30332. Email: russell.gentry@design.gatech.edu

Note. This manuscript was submitted on August 4, 2022; approved on January 28, 2023; published online on March 22, 2023. Discussion period open until August 22, 2023; separate discussions must be submitted for individual papers. This paper is part of the ***Journal of Composites for Construction***, © ASCE, ISSN 1090-0268.

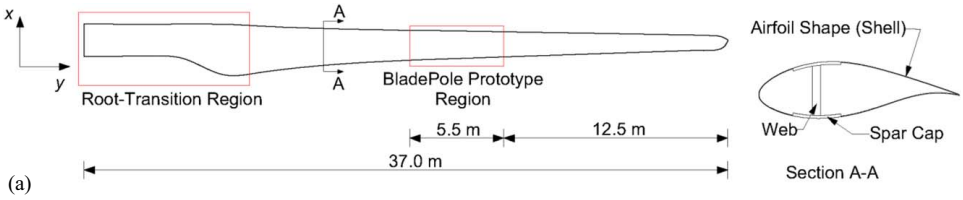

(a)

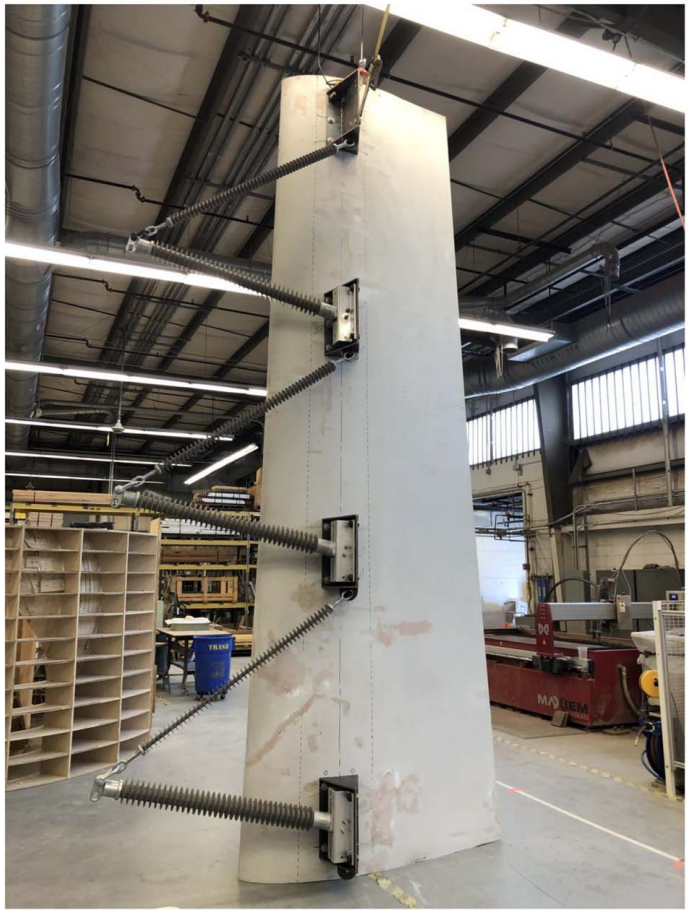

(b)

Fig. 1. (a) Visualization of a GE37 wind blade; and (b) BladePole prototype with three braced line posts attached to four universal connectors.

constructed in Cork, Ireland (CompositesWorld 2022; Ruane et al. 2022). A design for using wind blades as electricity transmission poles (also known as BladePoles) has been detailed by Alshannaq et al. (2021). Detailed testing of the properties of as-received wind blade material has been reported in Alshannaq et al. (2022). One of the major aspects needed to provide confidence in the BladePole design is ensuring that any new structural connections are adequate for transferring the expected loads to the wind blade in order to provide overall integrity to the structure.

The design of power transmission lines is based on a variety of safety aspects relating to the pole structure, including its structural integrity and fire safety, and the application of proper construction and maintenance plans. All parts of any power transmission line are designed with large safety margins in order to ensure a reliable power grid. In this study, we focused on detailed testing of the connections of the load-carrying appurtenances (e.g., insulators, crossarms, davits, guy wires, and posts) that bore the current-carrying electrical phases (typically, comprising either three or six phases) and the shield wires to the spar cap of a 1.5-MW GE37 wind blade to be used as a BladePole. Tests of pull-out and major- and minor-axis loading were performed in order to highlight the various limit states expected for the connection design. The spar cap is a thick GFRP component of the wind blade cross-section, mostly made of unidirectional composites up to 50 mm thick, with some ±45° and chopped strand mat (CSM) layers. The spar cap is the main load-bearing component that provides strength and stiffness to the overall wind blade. The layup in the spar cap of the GE37 wind blade studied herein was identified by burnout testing in the root-transition region by Alshannaq et al. (2022) as being $[(\pm 45)_2/\text{Mat}/0_n/(\pm 45)_2]$, where n = number of unidirectional layers. This stacking sequence was maintained throughout the length of the wind blade, up to the tip, with tapering in the number of layers. Other components include the aerodynamic shell, which causes the wind blade to rotate due to wind pressure, and the web (or webs), which provides structural stability to the cross-section against buckling and carries the shear forces it is subjected to during its operation. The GE37 examined was a single-web wind blade that had a total length of 37 m [see Fig. 1(a)] and was in service for 11 years at a wind farm in Langford, Texas. The blind bolting we analyzed related to the thick composite spar cap and not the sandwich-composite web or shell because these latter parts were not expected to provide sufficient connection strength. Therefore, all the major structural connections were made to the spar cap. In the mock-up [Fig. 1(b)], a set of three braced-line posts, supplied

J. Compos. Constr., 2023, 27(3): 04023024

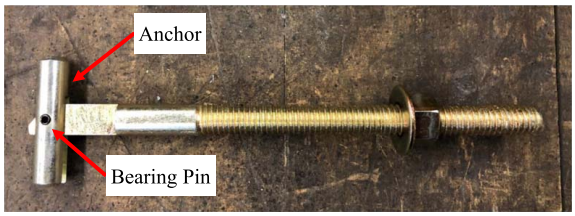

(a)

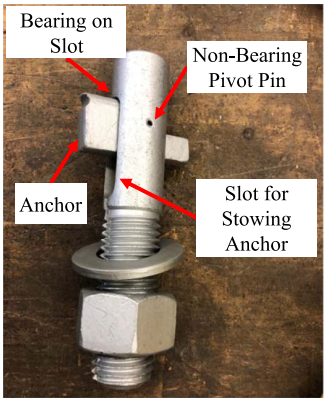

(b)

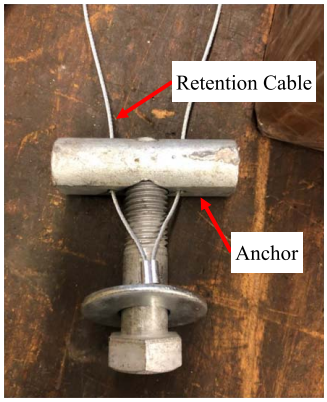

(c)

Fig. 2. Blind bolts used: (a) Type I; (b) Type II; and (c) Type III.

by Hubbell Power Systems, were installed using a custom adapter assembly, known as a universal connector. The braced-line post is a truss system that holds the (noninsulated) electrical conductors away from the surface of the pole and transfers the gravity and lateral loads from the electricity-carrying conductors [not depicted in Fig. 1(b)] to the structural load-carrying member as vertical loads (i.e., in the gravity direction) from the weight of the conductors, and as transverse loads (i.e., either in-plane or out-of-plane of the truss) from the wind load. The orientation of the loads with respect to the universal connector is shown in Fig. 13, in which it can be seen that the vertical loads result in major-axis loading and the transverse loads result in minor-axis loading.

Due to the nature of wind blade cross-sections (i.e., thin-walled, multicellular, and hollow), a specialized bolting system is necessary for connection to the wind blade. Such a specialized bolting method is used extensively in hollow steel sections and is typically known as blind bolting, where a bolt with a hidden anchor is inserted from the outside surface of the wind blade, and where the anchor, via a predefined movement, is deployed to bear on the inside surface of the wind blade without reaching the internal construction of the wind blade (see Fig. 2). In this study, we aimed to describe this blind-bolting method for FRP composites, in which only one side of the connection can be accessed.

Luo et al. (2013, 2016) investigated the performance of standard and blind bolts in joining tubular FRP components into space frame structures, connecting the FRP tubes to square hollow mild steel sections and testing these connections in tension and compression. Satasivam and Bai (2014) used standard and blind bolts to connect modular GFRP pultruded box beams and I-profiles to flat GFRP panels, which they tested through four-point bending. Their results showed a reduction in the mechanical performance of the blind-bolted connections compared with standard-bolted connections at the ultimate level, with 15% and 26% reductions in the ultimate tensile and compressive strengths, respectively (due to the slot in the blind bolt, which reduced the effective area of the bolt compared with a standard bolt) reported by Luo et al. (2016), and with a slight difference in the serviceability limit state (less than 10% variation in the initial stiffness) reported by Satasivam and Bai (2014). These results, combined with the ease of blind-bolt installation when access to both sides of the structural component is restricted, make blind bolts a good choice for connecting GFRP structural elements.

Wu et al. (2016) studied the effect of temperature increase on the behavior of double-lap pultruded FRP panel joints with standard and blind bolts, which might resemble the case for the proposed repurposing application (i.e., in the proposed application/s, a range of temperatures might be applicable, depending on the region where the structure is to be installed, thus the effect of temperature is important to consider, as it is with any composite material used in civil infrastructure). Wu et al.'s (2016) results confirmed that, on average, the maximum loads of the blind-bolted connections were 23% lower when compared with the standard-bolted connections due to the slot effect on the blind bolt's strength (see Fig. 2). In a comparative study on the difference between standard and blind bolts in double-lap joints of pultruded GFRP composites in static and fatigue tension, Wu et al. (2015) found that the use of blind bolts did not change the mode of failure when compared with the standard bolts (characterized here by shear-out failure), although the failure loads for the blind-bolted connections were slightly lower than for the standard-bolted connections. In the fatigue tests, the two types of bolt achieved similar fatigue lives, but with slightly reduced connection stiffness for the blind bolts.

It is important to reiterate that, in the literature, the major aspects of blind bolts that might influence connection strength have been highlighted, including the relative reduction in strength and stiffness when compared with standard bolts, and the possible premature failure of the bolt due to the reduced cross-sectional area of the bolt at the slot location. Also, the alignment of the anchor with the applied load direction has been recommended by Luo et al. (2013, 2016).

Our work focused on a mechanical characterization of the connections bolted to the thick (50 mm or more) GFRP spar cap of a decommissioned GE37 wind turbine blade to be repurposed in a second-life application (e.g., as a BladePole) because data in the literature concerning connections to thick GFRP materials are scarce and it is important to determine whether such connections are capable of transferring loads between various structural members. These composites were not designed to be joined using bolted connections in their first lives, and so they were studied to lay the groundwork for future repurposing applications that would require bolted connections. The experimental pull-out and bearing testing of the spar cap material is summarized in the following and compared with data from the literature on pultruded GFRP composites. The obtained data were then used to analyze and design a connection between a universal connector (i.e., a steel bracket that receives any type of connection) and the body of the repurposed wind blade. Different types of blind bolts were studied, and design recommendations, including safety factors, are emphasized.

Experimental Investigation

The research team had access to three widely used blind-bolt options (described in the following) with large bearing anchors inside. The size of the anchor was essential to the study because of the relatively low bearing and shear strength of the composite spar cap material (Alshannaq et al. 2022). Thus, the larger the anchor, the better the connection, thereby avoiding local damage and punching shear failure in the spar cap.

1. Type I blind bolt (McMaster-Carr 2022). This bolt was 9.5 mm in diameter × 152.4 mm in length. Even though this product had

a large bearing anchor (a solid cylinder) with dimensions of 38.1 mm × 9.5 mm, it bore a relatively small pin that failed at relatively low loads when using large tightening torques [see Fig. 2(a)].
2. Type II blind bolt (BlindBolt 2022). The M24 × 130 was 24 mm in diameter × 130 mm in length. This product provided an acceptable inside anchorage with sufficient bearing capacity, and bore, on the back side, a slot in the bolt, rather than a relatively small pin. The size of the anchor (a solid rectangle) was 8.9 mm × 48.3 mm [see Fig. 2(b)].
3. Type III blind bolt (RS Technologies Inc. 2022). This bolt was 19.1 mm in diameter × 82.6 mm in length. This product provided a good internal bearing capacity derived from the large bearing nut on the inside, with transfer of the load achieved through the bolt's threads. The size of the anchor (a solid cylinder) was 76.2 mm × 25.4 mm [see Fig. 2(c)].

After preliminary trials on these three blind bolts, Type I was eliminated due to its low load-carrying capacity [i.e., the anchor failed at a very low tightening torque, which was substantially below the 75 N·m recommended for suitable anchor bearing by the manufacturer of the Type II blind bolt (BlindBolt 2022)]. The Type II and Type III blind bolts were tested at coupon-scale for their pull-out and bearing properties, and were then used to fabricate full-sized connections for pull-out testing and major- and minor-axis loading in order to determine the ultimate capacity and the adequacy of the connection to resist the loads expected in the BladePole application.

Both coupon-scale and mesoscale testing was required to prove that the structural connections would be able to transfer loads (i.e., gravity loads from the weight of the conductors and transverse loads from wind pressure) between various structural members (e.g., braced-line post, universal connector, load-bearing spar cap) within appropriate safety margins. The testing procedures for, and limitations of, these connections are highlighted in the following.

Coupon-Scale Testing

The pull-out and bearing properties of the spar cap's thick unidirectional composite were required in order to determine the possible modes of failure in the proposed second-life application, bearing in mind that this composite was not intended to receive bolted connections in its first life.

Pull-Out Testing

Pull-out testing, per the guidelines in ASTM D7332 (ASTM 2016), was used to determine the pull-through capacity of the FRP-bolted connections. Even though this standard recommends a certain type of fixture for testing, any fixture could be affixed to the specimen for the application of a tensile load to pull the bolt through the FRP composite. The fixture used in this work is shown in Fig. 3(a) and was significantly larger than that described in the ASTM standard. A specimen on the testing machine bearing the fixture is shown in Figs. 3(b and c). The specimens were 139.7 mm × 139.7 mm × variable thicknesses, with a central-hole diameter of 25.4 + 1.6 mm. The variable thickness refers to the tapering of the spar cap along the length of the wind blade. Fig. 3(d) shows the orientation of the specimen with respect to the applied load [see Fig. 1(a) for orientation].

Two types of blind bolt were used—Type II, 24 mm in diameter, and Type III, 19.1 mm in diameter—with two spar cap thickness ranges (i.e., thin material, ranging from 25.4 to 35.6 mm—the thickness of the spar cap between 29 and 32 m from the root of the GE37—and a thick material, ranging from 40.6 to 55.9 mm—the thickness of the spar cap in the root-transition region of the GE37). Note that the hole's fixed dimension of 25.4 mm resulted in the Type III blind bolt being oversized because the anchor was 25.4 mm in diameter and had to be inserted into the 25.4-mm hole before inserting the bolt. Replicates of 10 specimens were used for each variable, resulting in a total of 40 tests.

The tests were performed on a 250-kN testing machine with 69-MPa-capacity hydraulic grips. A constant crosshead displacement of 0.635 mm/min was used, as specified in ASTM D7332 (ASTM 2016), with a gripping pressure of 41.4 MPa. This gripping pressure was used to ensure that no slippage occurred between the grips and the gripped steel in the fixture. It was decided to have a constant tightening torque of 75 N · m for both of the blind bolts based on a recommendation by the manufacturer of the Type II blind bolt (BlindBolt 2022). The Type III blind bolt pull-out specimens were not tightened to the same torque due to the presence of the long-threaded rod restricting the access of the socket on the torque wrench to the nut. However, it was thought that tightening would not affect the pull-out test results because the tension forces in the bolts overcame any precompression as the test progressed.

The modes of failure of representative specimens of the Type II and III blind bolts with thick and thin specimens are shown in Figs. 4 and 5, respectively. In these figures, the failure is shown from the top of the specimen [i.e., Figs. 4(a and d) and 5(a and d)], which is the outside surface of the wind blade, to the bottom of the specimen [(i.e., Figs. 4(b, c, e, and f) and 5(b, c, e, and f)], which is the inside surface of the wind blade, where the anchors go. Failure in the thick specimens for both types of blind bolts was characterized by failure of the anchor and superficial bearing damage to the FRP material. Failure in the thin specimens was characterized by bending of the anchor and excessive pull-through damage in the FRP material.

The load–deflection diagrams for the thick specimens with Type II and Type III blind bolts are shown in Figs. 6(a and b), respectively, and those for the thin specimens are shown in Figs. 6(c and d), respectively, with each plot having five replicates. Fig. 7 gives a comparison of the load–deflection curves of representative specimens of both types of blind bolt with the thin and thick spar cap specimens. It was found that the Type III blind bolt provided greater strength and stiffness to the connection because the anchor had larger dimensions. In addition, the deformation at failure (i.e., displacement) was comparable for both types of blind bolts. No significant difference was observed between the thin and thick spar caps with the Type III blind bolt. This was not the case for the Type II blind bolt, with the smaller anchor, and the thin spar cap material, with failure of the composite preceding failure of the anchor, thus giving a lower failure load,

The results obtained from the pull-out testing are summarized in Table 1. It is interesting to note that the thin specimens reached failure loads that were comparable to the full capacity of the blind bolts, especially the Type III blind bolt, and also that the thick specimens had failure in the blind bolt and, thus, reflected the capacity of the blind bolt.

Pin-Bearing Testing

Even though there are abundant data in the literature on the general pin-bearing of GFRP materials, data is scarce for thick (i.e., 50 mm and above) GFRP materials, and thus there was a need to determine the behavior of such thick GFRP materials (in this study, cut from a GE37 wind blade) in order to prove the efficacy of the proposed repurposing application, in which the bolts would be subjected to both pull-out and bearing loads.

The bearing capacities of the blind-bolted connections were obtained using ASTM D953 (ASTM 2019) based on the thickness of the composite material being tested. Pin-bearing tests were

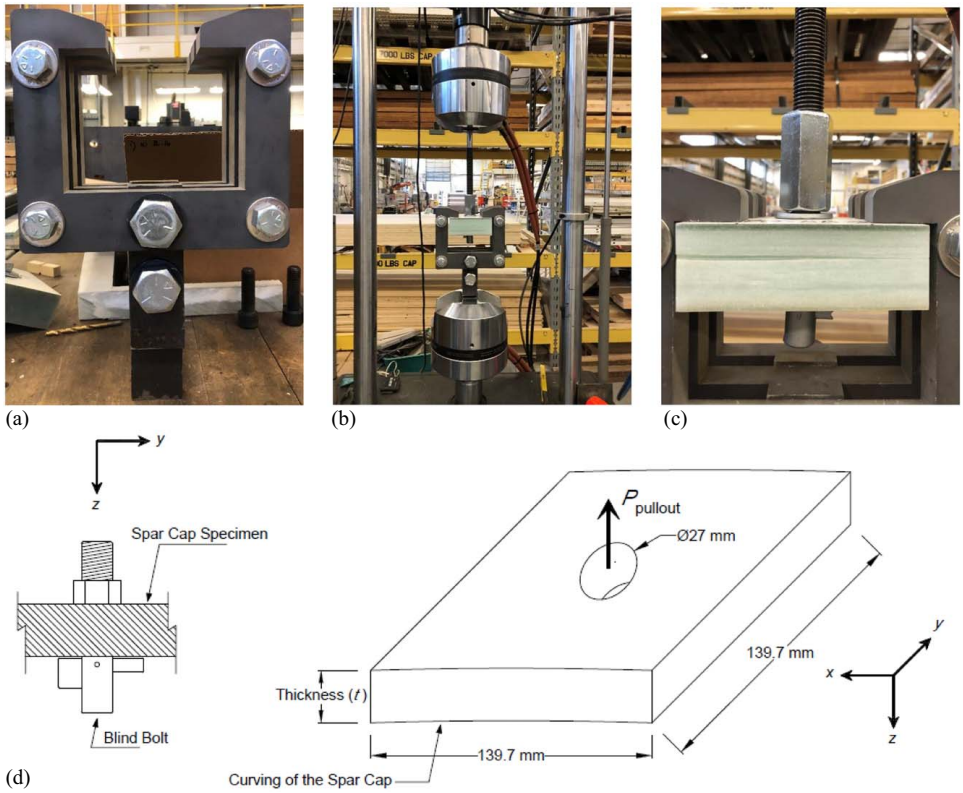

Fig. 3. Pull-out testing: (a) the fixture used; (b) a specimen attached to the fixture in the testing machine; (c) close-up of the specimen; and (d) orientation of the specimen and the blind bolt with respect to loading.

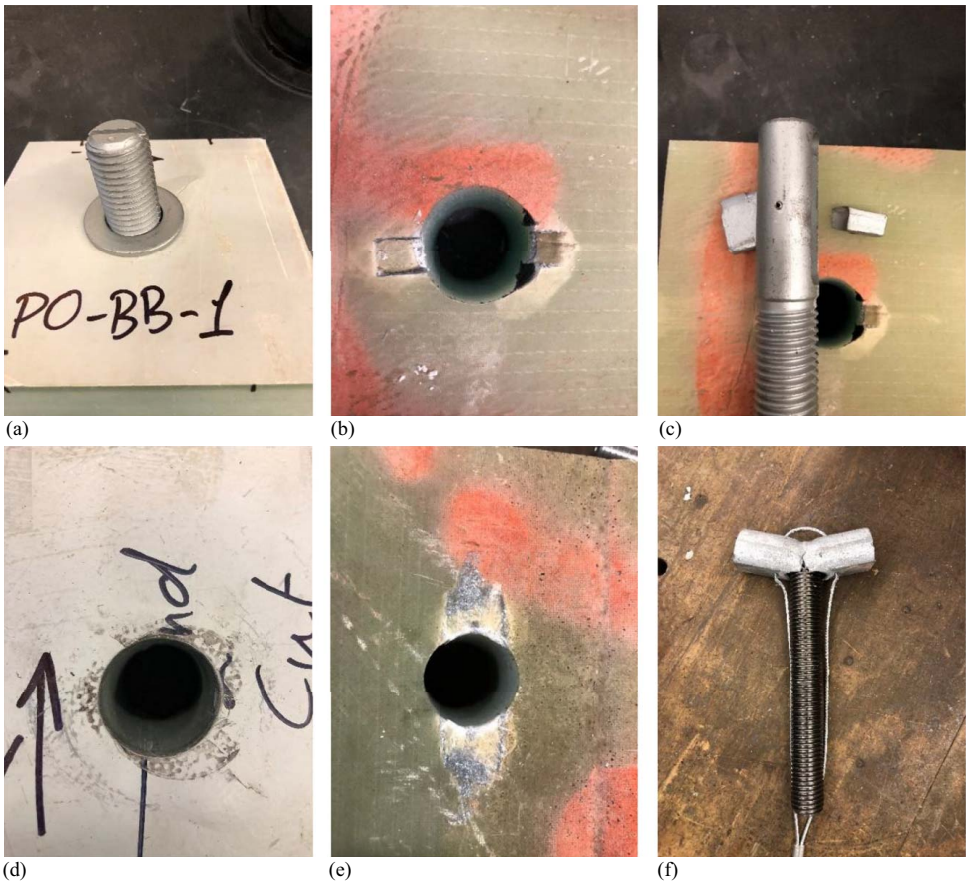

Fig. 4. Mode of failure of representative specimens: (a–c) thick Type II blind bolt; and (d–f) thick Type III blind bolt.

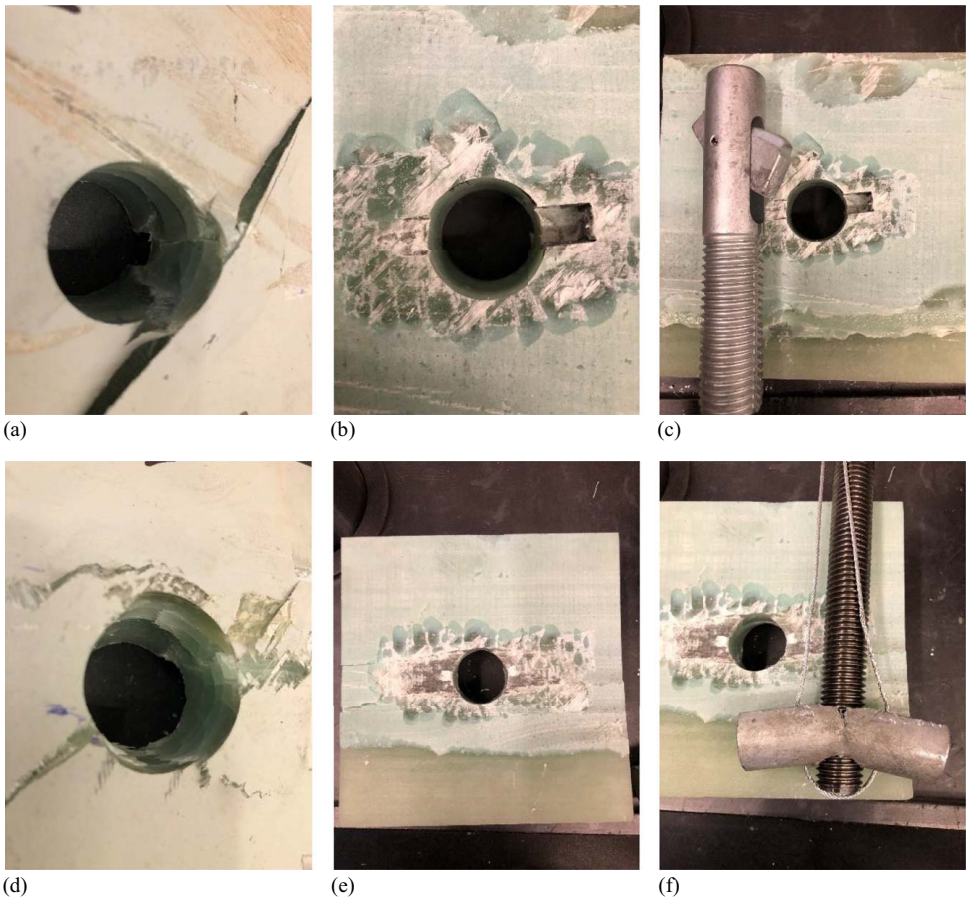

Fig. 5. Mode of failure of representative specimens: (a–c) thin Type II blind bolt; and (d–f) thin Type III blind bolt.

performed according to ASTM D953, Procedure C (ASTM 2019), with the pin-bearing fixture loaded in compression, as shown in Figs. 8(a and b). Fig. 8(c) shows the orientation of the specimen with respect to the applied load [see Fig. 1(a) for the orientation].

The pin-bearing specimens were 101.6 mm × 101.6 mm × variable material thickness, with a hole diameter of 25.4 + 1.6 mm. Two pin diameters were used—19.1 and 25.4 mm—with two orientations (i.e., longitudinal and transverse with respect to the

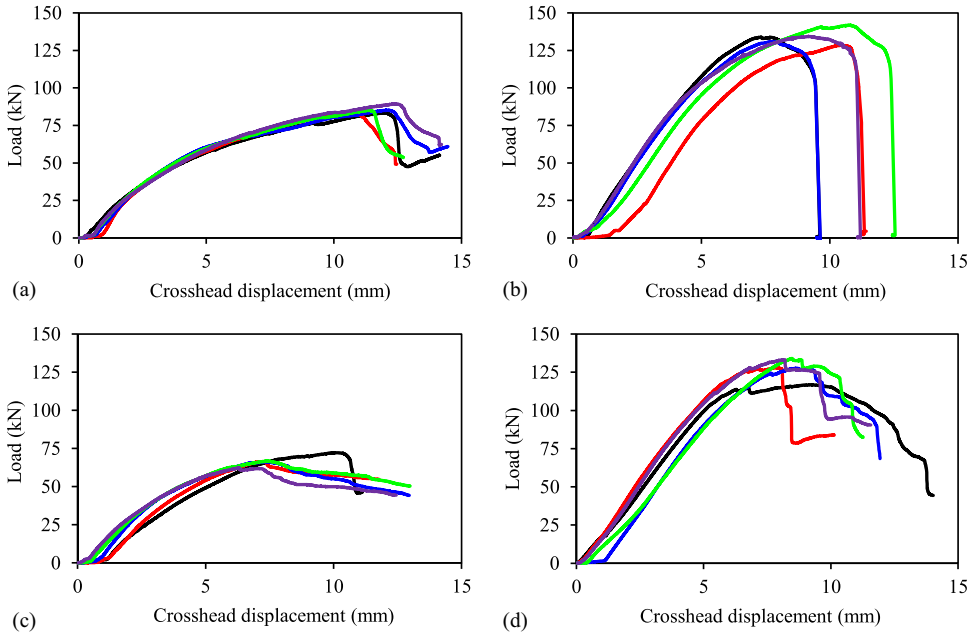

Fig. 6. Load–deflection curves for (a) Type II blind bolt with thick spar cap; (b) Type III blind bolt with thick spar cap; (c) Type II blind bolt with thin spar cap; and (d) Type III blind bolt with thin spar cap.

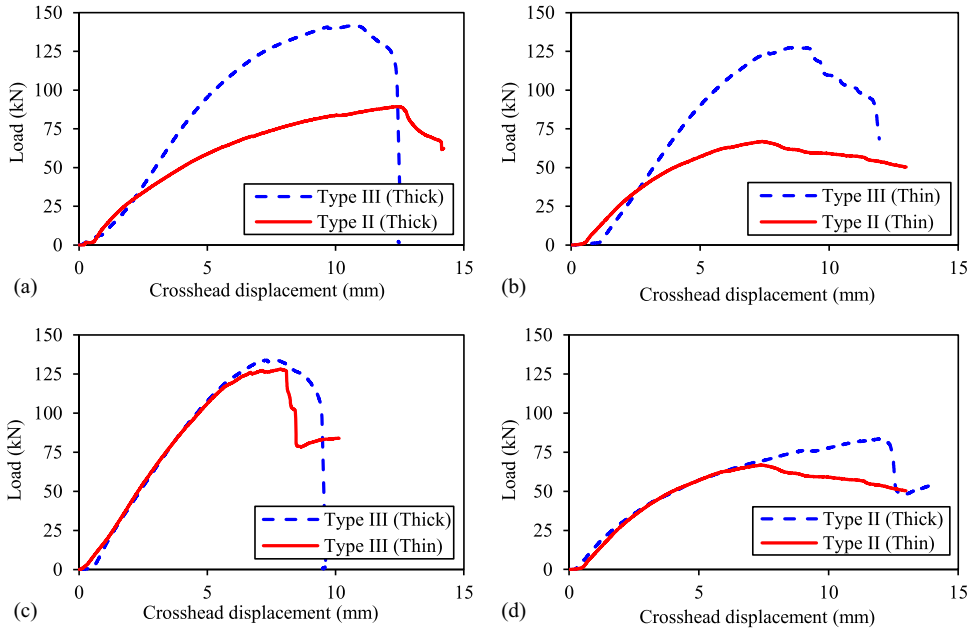

Fig. 7. Comparison between Type II and Type III blind bolts with (a) thick spar cap; and (b) thin spar cap; and comparison between thin and thick spar caps for the; (c) Type III blind bolt; and (d) Type II blind bolt.

wind blade reference axis). The spar cap thickness had a range of 22.9 to 38.1 mm, which was the material of the spar cap between 25 and 33 m from the root of the GE37. Replicates of 10 specimens were used for each variable, resulting in a total of 40 tests.

The tests were performed using a 250-kN testing machine with 69-MPa-capacity hydraulic grips. A constant crosshead displacement of 1.27 mm/min was used, as specified by ASTM D953 (ASTM 2019), with a gripping pressure of 41.4 MPa. This gripping pressure was used to ensure no slippage occurred between the grips and the steel gripped in the fixture.

The bearing stress was calculated using the equation $\sigma = P/td$, as provided in ASTM D953 (ASTM 2019), where σ = bearing stress; P = applied load; t = thickness; and d = pin diameter. ASTM D953 (ASTM 2019) does not have an equation for maximum bearing strain, and therefore the equation in ASTM D5961 (ASTM 2017a) was used for the bearing strain, $\varepsilon^{br} = \delta/d$, where ε^{br} = bearing strain; and δ = crosshead displacement. Both D953 and D5961 defined d as the hole diameter, which was defined as the pin diameter plus a specific clearance (here, 1.6 mm). But because the holes in this study had the same diameter, regardless of pin diameter (i.e., the specific clearance varied), it was decided to use the pin diameter to reflect the actual bearing properties of the material.

The mode of failure of representative specimens of the 19.1- and 25.4-mm diameters in both the longitudinal and transverse directions are shown in Figs. 9 and 10, respectively. The mode of failure for both diameters in the longitudinal direction was characterized by extensive bearing failure at the hole, followed by longitudinal cracks extending to the end of the specimen (these longitudinal cracks occurred after the ultimate load was reached with an increase in displacement). For both diameters in the transverse direction, the mode of failure was characterized by extensive bearing failure at the hole, followed by delamination of the layers (these interlaminar cracks occurred after the ultimate load was reached).

The bearing stress–strain diagrams of representative specimens with 19.1- and 25.4-mm pins in the longitudinal and transverse directions are shown in Figs. 11 and 12. In Fig. 11, the orientation was fixed and the pin diameter varied, whereas, in Fig. 12, the pin diameter was fixed and the orientation varied. It can be seen from Fig. 11 that the longitudinal bearing strength was almost the same, regardless of pin diameter. However, with increasing pin diameter in the transverse direction, the bearing strength increased. This could be due to the effect of oversized holes for the 19.1-mm pins resulting in a lower area of transverse fibers to bear on. Fig. 12 shows that the longitudinal bearing capacity was higher than the transverse bearing capacity for both pin diameters, and that the longitudinal stiffness was also higher than the transverse stiffness, which might be expected for mostly unidirectional FRP laminates (i.e., a GE37 spar cap).

The results obtained from the pin-bearing tests are summarized in Table 2. It was expected that these results would show some variations due to differences in the spar cap thickness causing slightly different fiber layups in different specimens, thus giving coefficient of variation values that were somewhat high (but still below 11%). The difference in thickness, from one specimen to another, resulted

Table 1. Summary of the pull-out testing results of the blind bolts

	Type II		Type III	
Attribute	Thick	Thin	Thick	Thin
Mean (kN)	84.5	65.6	131.5	130.4
SD (kN)	2.62	6.50	5.90	6.48
COV (%)	3.1	9.9	4.5	5.0
Mode of failure	Bolt failure + superficial material imprint	Material failure + anchor bending	Bolt failure	Material failure + anchor partial fracture

Note: SD = standard deviation; and COV = coefficient of variation.

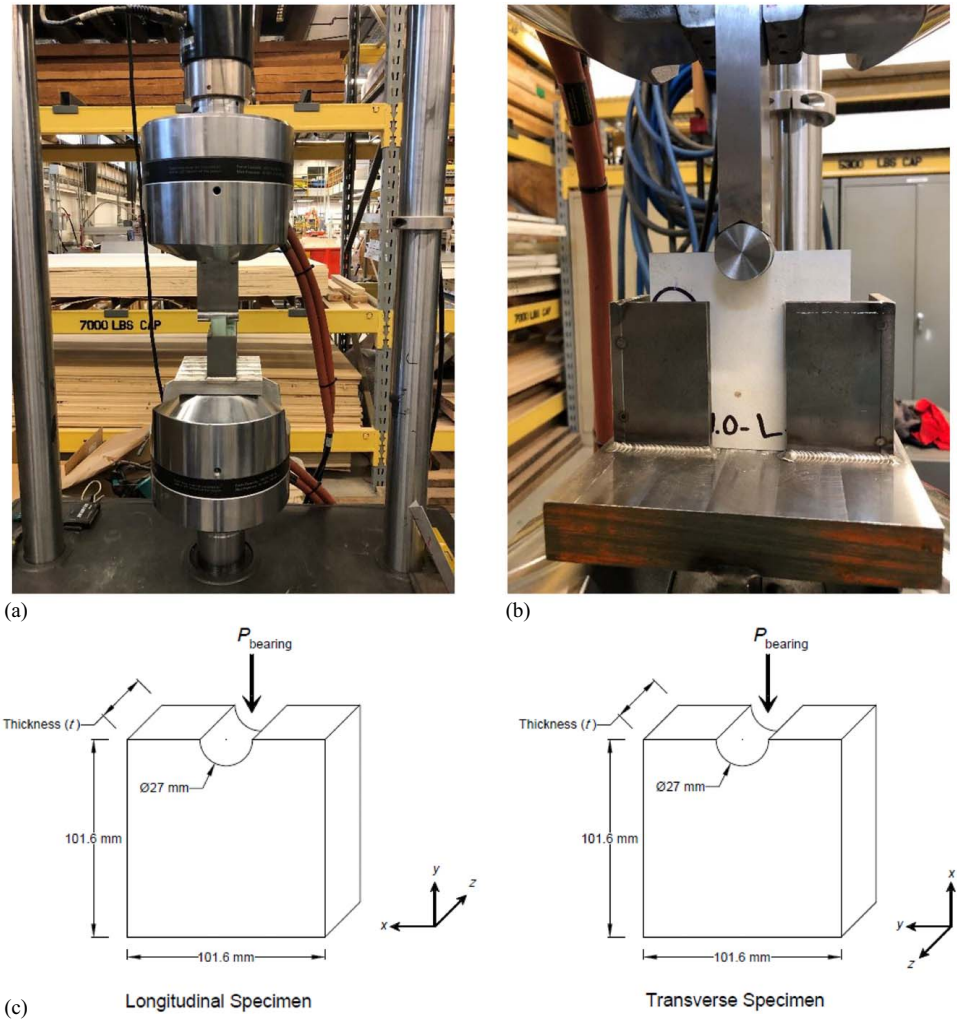

Fig. 8. Pin-bearing fixture: (a) side view; (b) front view; and (c) orientation of the specimen with respect to loading.

in a larger relative thickness for the 0° layers, which make the laminate more unidirectional.

Discussion of Test Results

Table 3 provides a summary of each tested property, with its corresponding characteristic value, obtained through ASTM D7290 (ASTM 2017b) and compared with two and three standard deviations from the mean. Even though these results were not going to be used for the numerical validation of the full connection testing (which was performed at full capacity, and thus would provide the ultimate values), these results could be used for future probability-based connection designs in order to incorporate proper material confidence levels.

The characteristic values confirmed the findings of Alshannaq et al. (2022) that ASTM D7290 (ASTM 2017b) provides comparable, and mostly lower, values when compared with three standard deviations from the mean. This gives a reasonable confidence level in relation to the typical three standard deviations from the mean of normally distributed data.

Table 4 provides a comparison of the pin-bearing results to data from the literature on pultruded FRP material used in civil infrastructure. It is interesting to note that the wind blade composites outperformed the pultruded FRP in terms of bearing properties even after 11 years of accumulated fatigue, which is due to the larger fiber weight fractions and the high-quality production by vacuum-assisted resin transfer molding (VARTM). It is important to mention that the results from the literature came from specimens with a diameter-to-thickness ratio of close to 1 and the tests presented herein had a ratio of ≤ 1. The spar cap pin-bearing capacities obtained herein were 1.1 to 1.6 times the literature data for pultruded FRP in the longitudinal direction and 0.9 to 1.7 times the literature data for the transverse direction. Even though the studied spar cap material was mostly unidirectional, the ±45° and CSM layers played an important role in enhancing the bearing strength in both the longitudinal and the transverse directions, with the superior VARTM processing of the wind blade materials relative to the pultrusion process, and the much higher volume fractions of the blade material versus the pultruded materials (which also had fillers), also contributing to the enhanced properties.

Proving that thick GFRP materials have bearing capacities that exceed the capacities of the widely used pultruded GFRP materials used in civil infrastructure is a valuable addition to the knowledge base on the design of connections for the unique shape of wind turbine blades. Pultruded materials have their own design standards that include procedures for bolted connections that can be designed for structural applications (ASCE Forthcoming), and thus the design of the thick GFRP spar cap materials can be assumed to have similar bearing behavior and design procedures (i.e., concerning the design of second-life applications).

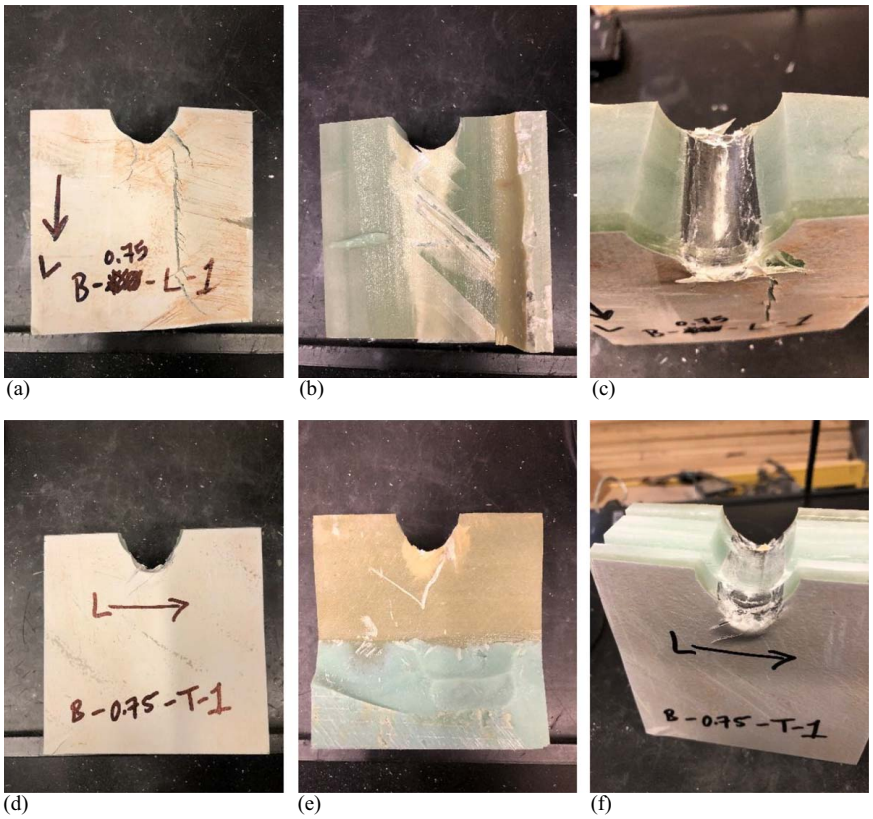

(a) (b) (c)

(d) (e) (f)

Fig. 9. Mode of failure of a representative 19.1-mm pin specimen: (a–c) in the longitudinal direction; and (d–f) in the transverse direction.

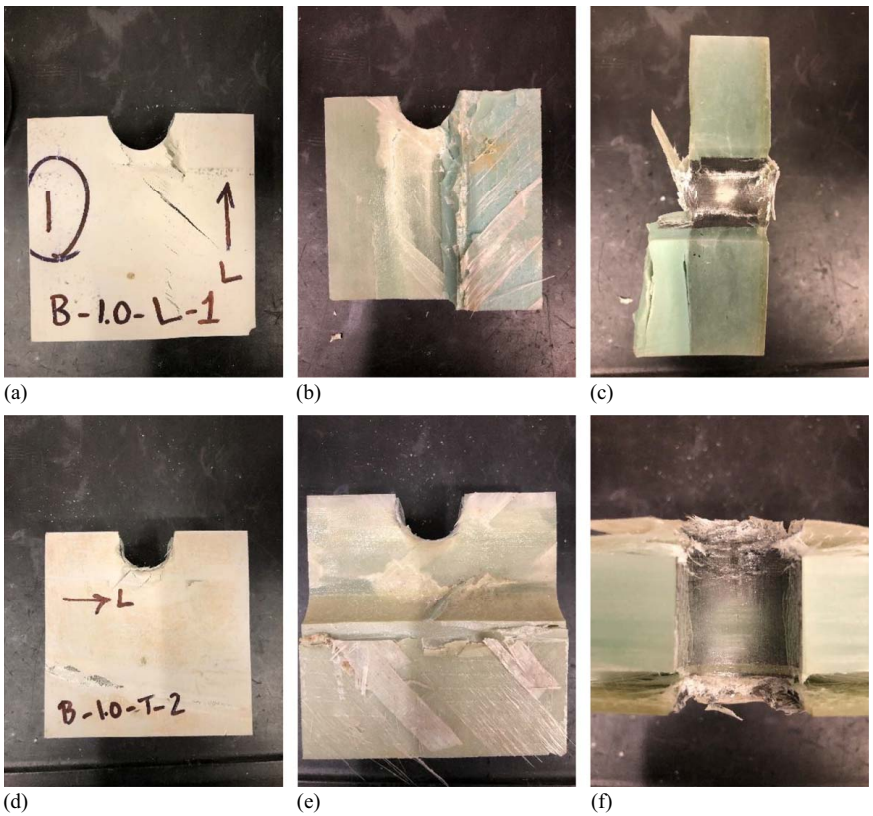

(a) (b) (c)

(d) (e) (f)

Fig. 10. Mode of failure of a representative 25.4-mm pin specimen: (a–c) in the longitudinal direction; and (d–f) in the transverse direction.

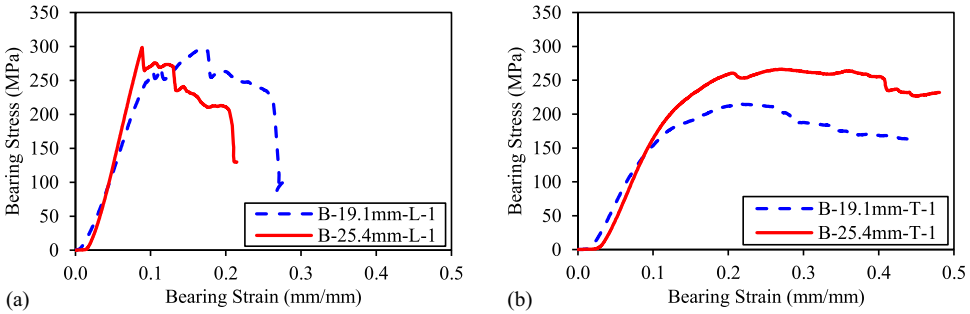

Fig. 11. Comparison between 19.1- and 25.4-mm pin diameters: (a) in the longitudinal direction; and (b) in the transverse direction (L = longitudinal; and T = transverse).

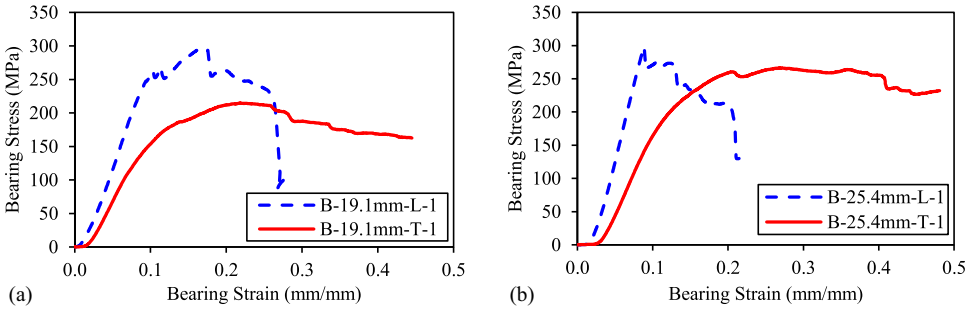

Fig. 12. Comparison between the longitudinal and transverse directions for a (a) 19.1-mm pin diameter; and (b) 25.4-mm pin diameter (L = longitudinal; and T = transverse).

Full Connection Testing

Various permutations of a steel universal connector connection bracket were proposed by the research team to be bolted to the spar cap material. The universal connector bracket was a combination of a base plate (to connect to the spar cap), a stem plate (to connect to the structure carrying the phases and conductors), and stiffening gusset plates, all made of Grade 50 steel. The final design of the universal connector is shown in Fig. 13. The base plate was 3.18 mm thick, while the stem plate and the two stiffeners were 9.53 mm thick, all welded together using 3.18-mm fillet weld. The universal connector was designed to resist similar loads to the ones presented by Alshannaq et al. (2021). It was also designed to receive the strut (i.e., the compressive member) of a braced-line post (which is an insulator assembly having two members, one carrying a tensile force and the other carrying a compressive force, forming a truss). The design philosophy was to obtain a universal connector that was strong when bending about the two main directions (i.e., the major and minor axes). This resulted in the stem plate and the two stiffener plates being 9.53 mm thick. However, the base plate was intended to conform to the wind blade's surface (i.e., to be bendable) while still being as thick as possible (i.e., to retain strength and stiffness). This trade-off resulted in a thickness of 3.18 mm. The purpose of the added semicircle was to be able to attach the tension member of the braced-line post to the other braced-line post connection on top of it. A picture of the BladePole prototype is shown in Fig. 1(b) (Al-Haddad et al. 2022).

Preparation of the specimens for testing involved cutting the spar cap into 609.6-mm-long blocks at the fullest width of the

Table 2. Summary of the pin-bearing testing results

	19.1-mm pin		25.4-mm pin	
Attribute	Longitudinal	Transverse	Longitudinal	Transverse
Mean (MPa)	302	212	296	246
SD (MPa)	17.4	9.50	32.2	10.3
COV (%)	5.8	4.5	11	4.2

Note: SD = standard deviation; and COV = coefficient of variation.

Table 3. Summary of the characteristic values for the connections blind bolted to the GE37 wind blade's spar cap compared with two and three standard deviations from the mean

Property	$\mu-2\sigma$	$\mu-3\sigma$	x_{char}	Status of x_{char} relative to $\mu-2\sigma$ and $\mu-3\sigma$
Pull-out of Type II blind bolt—thick (kN)	79.2	76.6	74.6	Lower
Pull-out of Type II blind bolt—thin (kN)	52.6	46.1	45.4	Lower
Pull-out of Type III blind bolt—thick (kN)	120	114	113	Lower
Pull-out of Type III blind bolt—thin (kN)	117	111	112	Between
Bearing of 25.4-mm pin—longitudinal (MPa)	232	199	201	Between
Bearing of 25.4-mm pin—transverse (MPa)	225	215	209	Lower
Bearing of 19.1-mm pin—longitudinal (MPa)	267	250	239	Lower
Bearing of 19.1-mm pin—transverse (MPa)	193	183	186	Between

Note: μ = mean; σ = standard deviation; and x_{char} = characteristic value.

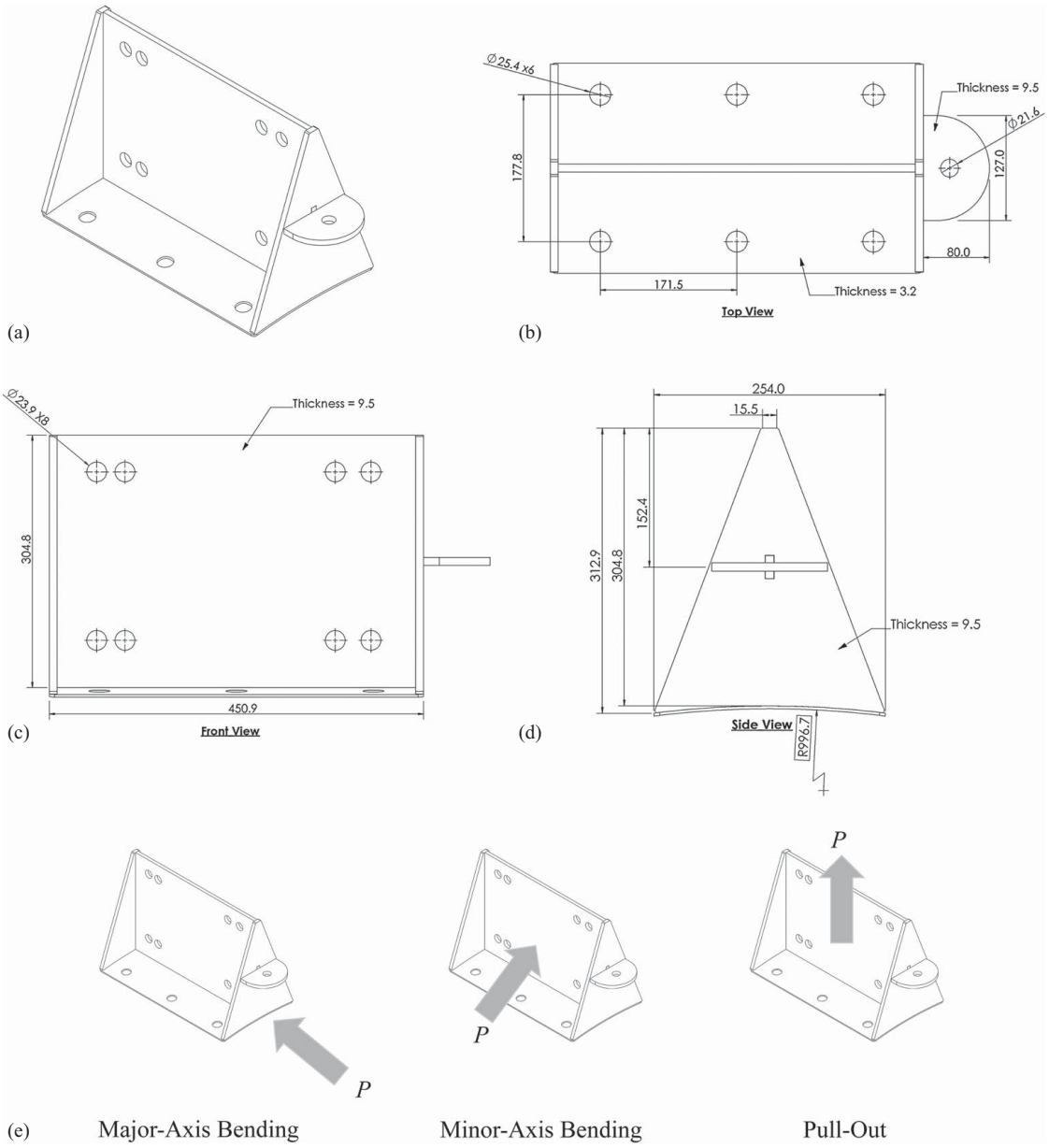

Fig. 13. Details of the universal connector: (a) isometric drawing; (b) top view; (c) side view; (d) front view; and (e) loading directions (all dimensions are in mm).

spar cap using a carbon-tipped circular saw. The holes for bolting were cut using a waterjet. The whole test article was attached to a strong steel wall. In all specimens, the anchor of the blind bolt was aligned parallel to the longitudinal axis of the wind blade (i.e., the reference axis). This orientation was suggested by data in the literature and because the inside surface of the spar cap tapered more significantly in the transverse direction, which would have prevented the proper bearing of the anchor if it was aligned with the transverse direction (this alignment plan was also implemented on the bolted coupon testing done earlier). Similar to the bolted coupon testing, the universal connector bolt holes in the spar cap were $25.4 + 1.6$ mm for both the Type II and III blind bolt specimens. All tests were performed using a 445-kN load cell attached to a 334-kN actuator controlled by a controller that was connected to a data acquisition system for acquiring simultaneous load and displacement data (displacement data represented the movement of the actuator).

Major-Axis Testing

The importance of major-axis testing originated from the fact that the universal connector in the BladePole application will be subjected to major-axis loading through the shear forces (i.e., the gravity loads) of the assembly. These shear forces would transfer into the bending moment on the base plate because the center of the connection would be at the mid-height of the stem plate [see Fig. 13(e)].

A simplified visualization of the fixture used for testing the major-axis capacity of the universal connector is shown in Fig. 14(a). For the major-axis testing, the load was applied at 165.1 mm from the base plate (close to the mid-height of the stiffener plate). Fig. 14(b) shows the test article with a Type III blind bolt. The load was applied directly from the load cell with the help of a 69.8-mm-diameter circular plate that articulated on a spherical bearing in order to reduce the shear force transmitted to the load cell. The test article was attached to the strong steel wall with 11×19.1-mm threaded rods all around.

Table 4. Comparison of experimental pin-bearing results to data from the literature

	GE37		After Matharu and Mottram (2017)[a]	After Mottram and Zafari (2011)[b]	After Creative Pultrusion (2022) – 1500/1525[c]		After Creative Pultrusion (2022) – 1625[c]	
Material/location	spar cap		flange	web	flange	web	flange	web
Fiber content by mass (%)	68[d]		50[c]	50[c]	50[c]		50[c]	
Longitudinal bearing strength								
Pin diameter (d_b) (mm)	19.1	25.4	9.81	9.7	—	—	—	—
Mean (MPa)	302	296	210	188	228	234	262	269
SD (MPa)	17.4	32.2	19.9	6.2	—	—	—	—
COV (%)	5.8	11	9.5	3.3	—	—	—	—
Transverse bearing strength								
Mean (MPa)	212	246	142	168	159	207	183	238
SD (MPa)	9.50	10.3	5.31	10.5	—	—	—	—
COV (%)	4.5	4.2	3.8	6.2	—	—	—	—

Note: SD = standard deviation; and COV = coefficient of variation. All tests done according to ASTM D953 (ASTM 2019).
[a]After Matharu and Mottram (2017), plain pin-bearing, $d/t = 0.98–1$, flange = 254 × 254 × 9.53 mm, wide flange shape of the Creative Pultrusion 1525 series.
[b]After Mottram and Zafari (2011), $d/t = 1.06–1.07$, web = 203 × 203 × 9.53 mm, wide flange shape of the Creative Pultrusion 1525 series.
[c]After Creative Pultrusion (2022) Pultex Fiber-Reinforced Polymer SuperStructural Profiles.
[d]According to tests done by Alshannaq et al. (2022).

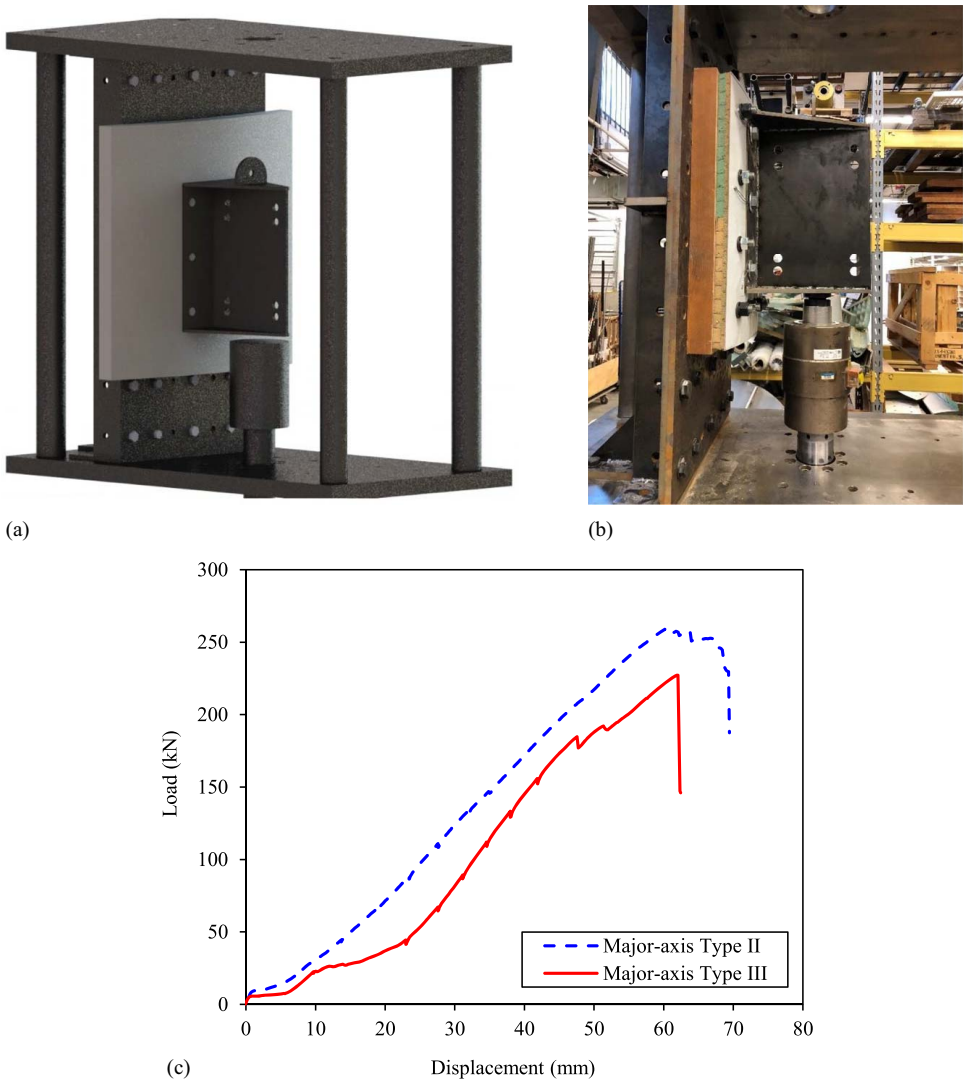

Fig. 14. Major-axis testing: (a) visualization of the fixture; (b) major-axis fixture with Type III blind bolts; and (c) load–deflection curves for major-axis testing.

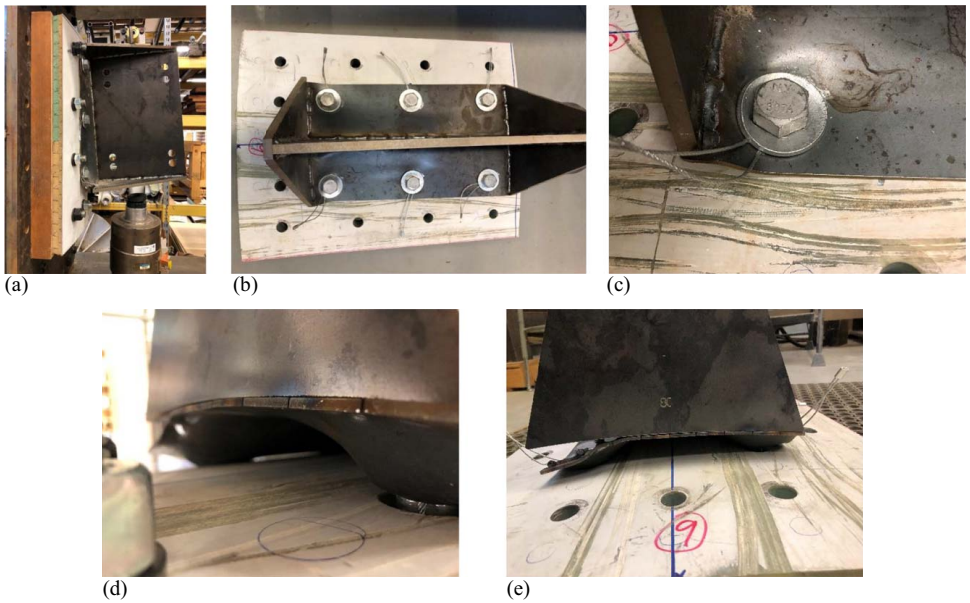

Fig. 15. Failure of Type III blind bolt major-axis specimen: (a) welding failure and excessive deflection; and (b–e) buckling and welding fracture of the base plate.

Fig. 16. Failure of Type II blind bolt major-axis specimen: (a) welding failure and excessive deflection; and (b and c) buckling and welding fracture of the base plate.

The load was applied at a constant rate of 3.81 mm/min in compression (i.e., the load was applied upward). Load-displacement curves were constructed for each specimen, and are shown in Fig. 14(c) for both the Type II and Type III blind bolts. As can be seen, the overall behavior of the Type II and Type III blind bolts was similar, with a slight increase in stiffness for the Type II specimen due to the larger nuts used, which provided enhanced support for the thin base plate. It is important to note that the behavior at the beginning of the test was not similar due to sliding of the blind bolts in their holes (the hole sizes were the same, but the bolts had different sizes) and the recess of the test fixture. When comparing the pull-out tests performed previously to these full connection load capacities on major-axis bending, and using simple moment calculations, the resultant pull-out load for each of the Type III blind bolts (in tension) was 54.6 kN, and for each of the Type II blind bolts (in tension) it was 62.6 kN. For the failure loads observable in Fig. 14(c), these represent 42% of the Type III and 74% of the Type II blind bolts' pull-out capacities, as presented in Table 1. The mode of failure of the two specimens was characterized by excessive bending of the base plate and welding failure in the region close to the applied load (i.e., subjected to tensile stresses from bending). These modes of failure are shown in Fig. 15 for the Type III blind bolt and Fig. 16 for the Type II blind bolt.

Minor-Axis Testing

The importance of the minor-axis testing originated from the fact that the universal connector would be subjected to minor-axis loading through the compressive force in the strut of the braced-line post, the compressive force being exerted as shear forces on the universal connector, which would be transferred as the bending moment on the base plate because the center of the connection would be at the mid-height of the stem plate [see Fig. 13(e)].

A simplified visualization of the fixture used for testing the minor-axis capacity of the universal connector is shown in Fig. 17(a). For the minor-axis testing, the load was applied at 165.1 mm from the base plate (close to the mid-height of the stem plate). Fig. 17(b) shows the test article with a Type III blind bolt. Similarly to the major-axis testing, the load was applied directly from the load cell by introducing a 69.8-mm-diameter circular plate, which articulated on a spherical bearing, to reduce the shear force transmitted to the load cell. The test article was attached to the strong steel wall with 16 × 19.1-mm threaded rods all around.

The load was applied at a constant rate of 3.81 mm/min in compression (i.e., the load was applied upward). Load-displacement curves were constructed for each specimen and are shown in Fig. 17(c) for both the Type II and III blind bolts. As can be seen, the behavior was similar for both specimens. Like the

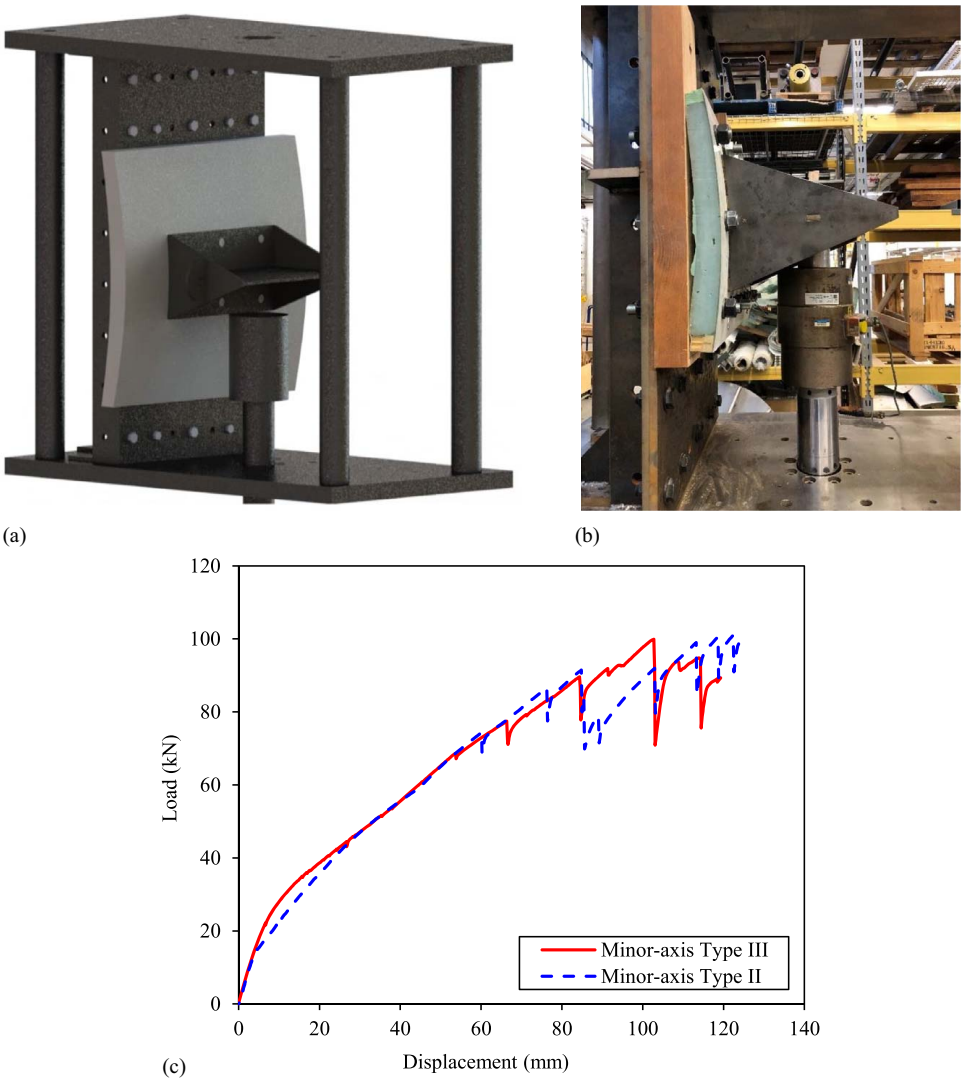

Fig. 17. Minor-axis testing: (a) visualization of the fixture; (b) minor-axis fixture with Type III blind bolts; and (c) load–deflection curves for minor-axis testing.

major-axis testing, the behavior at the beginning of the test was dissimilar due to sliding of the blind bolts in their holes (the hole sizes being the same, but the bolts having different sizes) and the recess of the test fixture. The tests were stopped after the full stroke of the actuator was reached at 127 mm. When comparing the pull-out tests performed previously to these full connection load capacities on minor-axis bending, and using simple moment calculations, the resultant pull-out load for each of the Type III blind bolts (in tension) was 30.9 kN, and for each of the Type II blind bolts (in tension) it was 31.3 kN for the failure loads that can be seen in Fig. 17(c). These were 24% of the Type III blind bolt's pull-out capacity and 37% of the Type II blind bolt's pull-out capacity, as presented in Table 1. The mode of failure was characterized by excessive deformation of the stem and stiffener plates, coincident with welding fracture and pull-out of the blind bolts through the thin base plate. The mode of failure is shown in Fig. 18 for the Type III blind bolt and Fig. 19 for the Type II blind bolt.

Pull-Out Testing

The importance of the pull-out testing originated from the fact that the universal connector would be subjected to pull-out loading through the effect of wind loads along the direction of the power line. Even though these loads were expected to be minimal, a capacity check was required to determine reliable safety levels.

A simplified visualization for testing the pull-out capacity of the universal connector is shown in Fig. 20(a), whereas Fig. 20(b) shows the test article with Type II blind bolts. As can be seen, the test fixture involved attaching the stem plate of the test article to the load cell using four vertical plates (two on each side) that were 12.7 mm thick, welded to a 12.7-mm-thick steel C-section that had a 50.8-mm-diameter central hole for a threaded rod to go through and be attached to the load cell. The four vertical plates had the same hole pattern as the stem plate, and this pattern was dependent on the braced-line post pattern from the manufacturer (in the current case, these holes were 23.9 mm in diameter). The test article was attached to the steel frame using 4×25.4-mm and 4×15.9-mm threaded rods.

The load was applied at a constant rate of 3.81 mm in tension (i.e., the load was applied downward). Load-displacement curves were constructed for each specimen and are shown in Fig. 20(c) for both the Type II and III blind bolts. As can be seen, there was a slight difference in the full capacity. However, the first two major drops with the Type III blind bolt specimen occurred earlier than with the Type II blind bolt specimen. These were due to

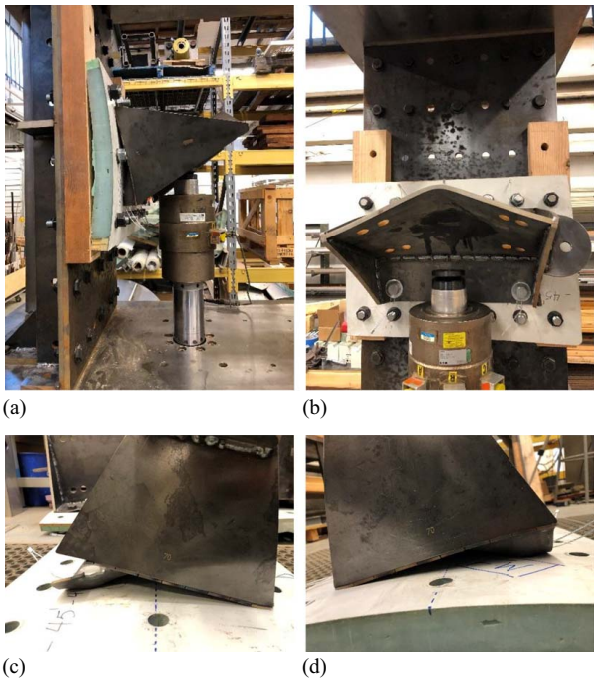

Fig. 18. Failure of Type III blind bolt minor-axis specimen: (a) welding failure and excessive deflection; (b) bending of the stem and stiffener plates; and (c and d) welding failure and excessive bending of the base plate.

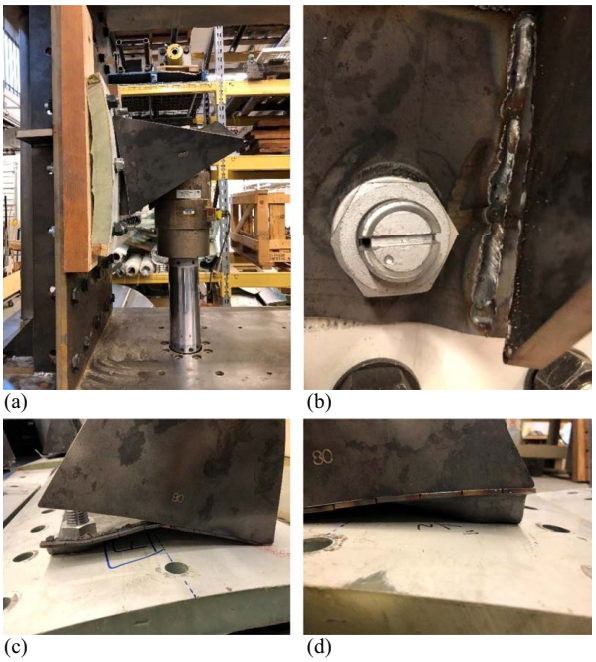

Fig. 19. Failure of Type II blind bolt minor-axis specimen: (a) welding failure and excessive deflection; and (b–d) bending and welding fracture of the base plate at the blind bolt location.

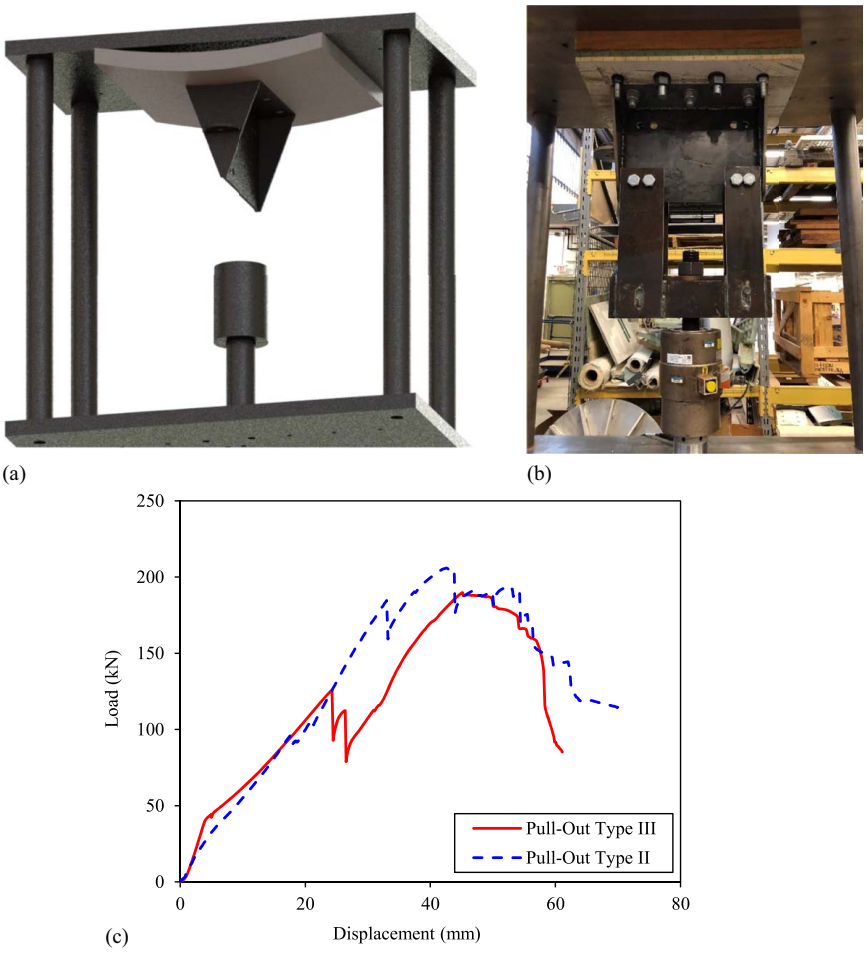

Fig. 20. Pull-out testing: (a) visualization of the fixture; (b) pull-out fixture with Type II blind bolts; and (c) load–deflection curves for pull-out testing.

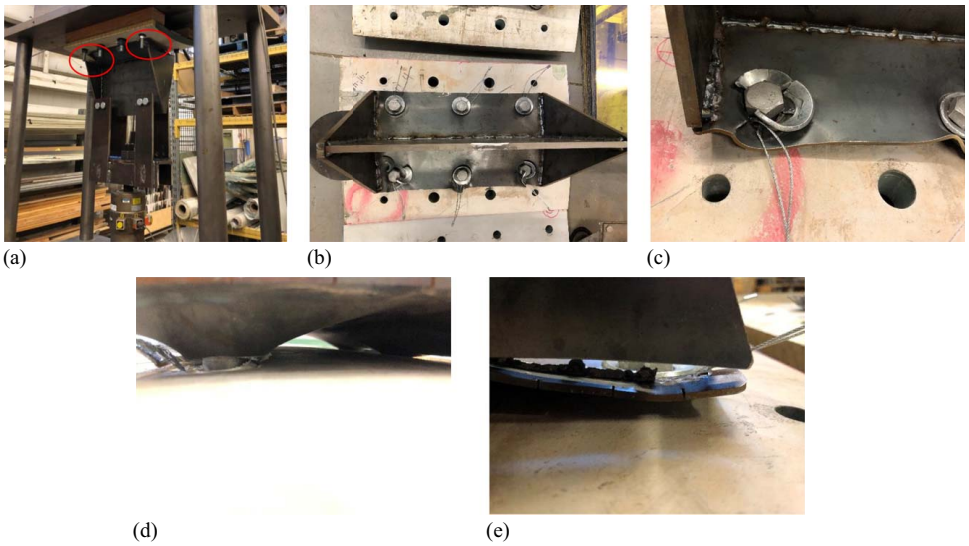

Fig. 21. Failure of Type III blind bolt pull-out specimen: (a) welding failure on the same side of the universal connector; and (b–e) buckling and welding fracture of the base plate.

welding fracture, which occurred at the base–stiffener-plate welding and on the same side of the universal connector (see Fig. 21). The same welding failure occurred with the Type II blind bolt specimen, but it occurred later and on two opposite sides (see Fig. 22), and thus there was no excessive drop in capacity when compared with the Type III blind bolt. The final failure for both specimens was characterized by welding failure and eventual pull-out failure in the bolt–base-plate region. The slight increase in ultimate capacity of the Type II blind bolt was attributed to the larger nuts used with the bolts, which provided better support to the thin base plate. When comparing the pull-out tests completed previously with these full connection load capacities in pull-out, and when dividing the failure load by the number of blind bolts, the resultant pull-out load for each of Type III blind bolt was 31.7 kN, and for each of the Type II blind bolts, it was 34.3 kN for the failure loads observed in Fig. 20(c). These were 24% of the Type III blind bolt's pull-out capacity and 41% of the Type II blind bolt's pull-out capacity, as presented in Table 1. It is important to note that the behavior at the beginning of the test was not similar due to sliding of the blind bolts in their holes (the hole sizes were the same, but the bolts had different sizes) and the recess of the test fixture.

Results Analysis and Discussion

Table 5 summarizes the results obtained from the full connection testing. It also provides the safety factors for both the Type II and III blind bolts, if the connection is used to resist a vertical load of 22.2 kN on the truss (i.e., the braced-line post), which is the load case of concurrent wind at 48.3 km/h and ice accumulation of 19.1 mm on the conductors (i.e., this would result in a vertical load "major-axis case" of 22.2 kN and a horizontal load "minor-axis case" of 23.2 kN). These loads were obtained when modeling a right-angled truss with a height of 2.93 m (i.e., the spacing between the universal connectors) and a horizontal length (i.e., length of the compression member) of 3.05 m. It is important to note that

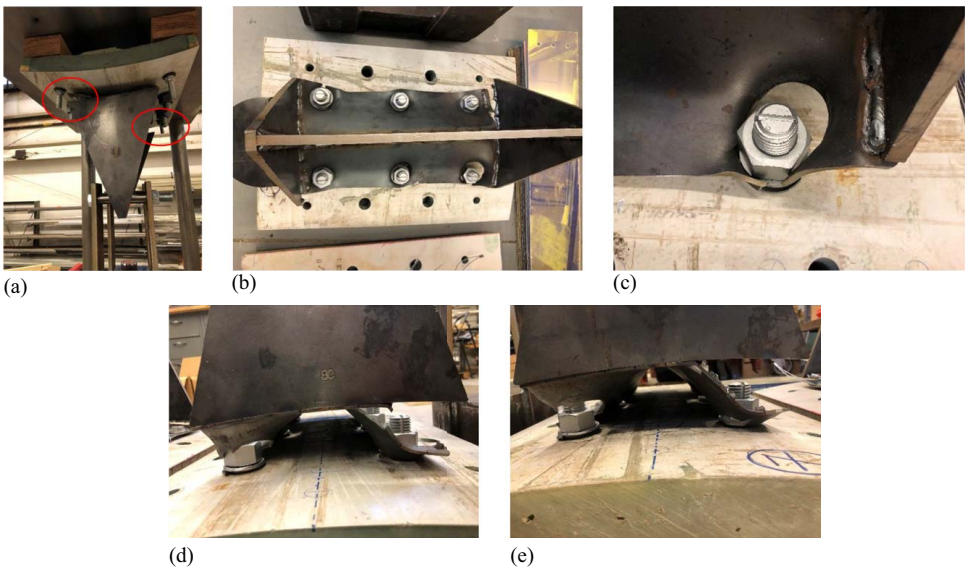

Fig. 22. Failure of Type II blind bolt pull-out specimen: (a) welding failure on opposite sides of the universal connector; and (b–e) buckling and welding fracture of the base plate.

J. Compos. Constr., 2023, 27(3): 04023024

Table 5. Safety factors of full connection testing using different types of blind bolts

Property	Type III (kN)	Type II (kN)	Demand (kN)	Type III (SF)	Type II (SF)
Major axis	227	260	22.2	10	12
Minor axis	99.9	101	23.2	4.3	4.4
Pull-out	190	206	—	—	—

Note: SF = safety factor.

any truss shape and dimensions could be used to obtain the respective safety factors of the final product based on the testing results presented here.

Conclusions

In this study, we investigated the capacity of connections bolted to the spar cap of a decommissioned GE37 wind turbine blade. The following conclusions were drawn from the results:

- Both the Type II and III blind bolts provided promising pull-out strength and stiffness values for bolted connections in thick FRP composites where access to one side is difficult (e.g., hollow cross-sections), with the Type III blind bolt providing more pull-out strength and stiffness due to the size of its internal anchor. The Type III blind bolt's pull-out strength was characterized as being 1.5 to 2 times the strength of the Type II blind bolt.
- The pull-out capacity of the connections blind bolted to the spar cap of the GE37 wind blade provided insights into both the pull-out strength of the blind bolt and of the spar cap composite. The pull-out strength of the blind bolt was determined through testing thick (i.e., ranging from 40.6 to 55.9 mm) spar cap specimens, while the pull-out strength of the spar cap composite was determined through the testing of thin (i.e., ranging from 25.4 to 35.6 mm) specimens.
- The single-shear tests widely used to characterize the bearing capacity of bolted connections were not applicable to the thick (i.e., reaching ~50 mm) GFRP spar cap material of the GE37 because of the large bending stresses introduced by the eccentricity during load application. Consequently, ASTM D953 Procedure C (ASTM 2019), with the pin-bearing fixture, was more suited to these composites.
- The spar cap pin-bearing capacities were 1.1 to 1.6 times the data from the literature for pultruded FRP in the longitudinal direction, and 0.9 to 1.7 times the literature data in the transverse direction.
- No effect of pin size on the bearing strength was observed for the thick unidirectional laminates in the longitudinal direction (i.e., the spar cap of the GE37). However, the effect was pronounced in the transverse direction, with a 16% increase in bearing strength observed from changing the pin diameter from 19.1 to 25.4 mm. This is true, given that the hole diameter was fixed at 25.4 + 1.6 mm, which was a necessity in using the Type III blind bolt.
- A steel universal connector was designed and tested for possible use in second-life applications of decommissioned wind turbine blades (e.g., BladePoles, BladeBridges). The testing of the major and minor axes, and the pull-out capacities provided good safety margins when compared with the load cases expected for BladePole application, resulting in a minimum safety factor of 4.3 when a vertical gravity load of 22.2 kN is applied to a braced-line post. Steel yielding and welding fracture modes of failure were observed, which suggested increasing the amount of welding (i.e., on both sides of the steel plates), which would postpone this mode of failure and result in more-favorable steel yielding.
- The Type III blind bolts would need to be installed in oversized holes due to the fact that the anchor is a rod with a diameter of 25.4 mm while the bolt is 19.1 mm in diameter. This would result in connection slip as the load was applied, and it might result in secondary loads or moments on the universal connector, thus needing to be taken into consideration at the design stage.

The authors would like to emphasize that this work was intended to prove that structural connections are possible even with the unique shape of wind blades, and that this paper is only one step towards a more-extensive analytical and numerical study of these connections in a final prototype, which will account for various field conditions during the service life of the repurposed structure.

Data Availability Statement

All data, models, or code that support the findings of this study are available from the corresponding author upon reasonable request.

Acknowledgments

Support for this research was provided by the National Science Foundation (NSF) under Grants 2016409, 1701413, and 1701694, by InvestNI/Department for the Economy (DfE) under Grant 16/US/3334, and by the Science Foundation Ireland (SFI) under Grant USI-116 as part of the US–Ireland tripartite research program.

The authors would like to thank the Logisticus Group of Greenville, South Carolina, for supplying the spar cap specimens for testing and Hubbell Power Systems for supplying the braced-line posts.

References

Al-Haddad, T., A. Alshannaq, L. Bank, M. Bermek, R. Gentry, Y. Henao-Barragan, S. Li, A. Poff, J. Respert, and C. Woodham. 2022. "Strategies for redesigning high performance FRP wind blades as future electrical infrastructure." In *ARCC-EAAE 2022 Int. Conf. – Resilient City: Physical, Social, and Economic Perspectives*. San Antonio, TX: Architectural Research Centers Consortium, Inc.

Alshannaq, A. A., L. C. Bank, D. W. Scott, and T. R. Gentry. 2021. "Structural analysis of a wind turbine blade repurposed as an electrical transmission pole." *J. Compos. Constr.* 25 (4): 04021023. https://doi.org/10.1061/(ASCE)CC.1943-5614.0001136.

Alshannaq, A. A., J. A. Respert, L. C. Bank, D. W. Scott, and T. R. Gentry. 2022. "As-received physical and mechanical properties of the spar cap of a GE37 decommissioned GFRP wind turbine blade." *J. Mater. Civ. Eng.* 34 (10): 04022266. https://doi.org/10.1061/(ASCE)MT.1943-5533.0004410.

ASCE. Forthcoming. *Load and resistance factor design (LRFD) for pultruded fiber reinforced polymer (FRP) structures*. Reston, VA: ASCE.

ASTM. 2016. *Standard test method for measuring the fastener pull-through resistance of a fiber-reinforced polymer matrix composite*. ASTM-D7332. West Conshohocken, PA: ASTM.

ASTM. 2017a. *Standard test method for bearing response of polymer matrix composite laminates*. ASTM-D5961. West Conshohocken, PA: ASTM.

ASTM. 2017b. *Standard practice for evaluating material property characteristic values for polymeric composites for civil engineering structural applications*. ASTM-D7290. West Conshohocken, PA: ASTM.
ASTM. 2019. *Standard test method for pin-bearing strength of plastics*. ASTM-D953. West Conshohocken, PA: ASTM.
Bank, L., E. Delaney, J. Mckinley, R. Gentry, and P. Leahy. 2021. "Defining the landscape for wind blades at the end of service life". Accessed November 9, 2022. https://www.compositesworld.com/articles/defining-the-landscape-for-wind-blades-at-the-end-of-service-life.
Bank, L. C. 2006. *Composites for construction: Structural design with FRP materials*. Hoboken, NJ: Wiley.
BlindBolt. 2022. "Blind bolt product specification Geomet 500B – Property Class 10.9 – GBB24130DTASM – M24X130." Accessed November 9, 2022. https://www.blindbolt.co.uk/the-blind-bolt/technical-data/.
Brøndsted, P., H. Lilholt, and A. Lystrup. 2005. "Composite materials for wind power turbine blades." *Annu. Rev. Mater. Res.* 35 (1): 505–538. https://doi.org/10.1146/annurev.matsci.35.100303.110641.
Chen, J., J. Wang, and A. Ni. 2019. "Recycling and reuse of composite materials for wind turbine blades: An overview." *J. Reinf. Plast. Compos.* 38 (12): 567–577. https://doi.org/10.1177/0731684419833470.
CompositesWorld. 2022. "Re-wind network successfully installs repurposed wind blade pedestrian bridge." Accessed April 25, 2022. https://www.compositesworld.com/news/re-wind-network-successfully-installs-repurposed-wind-blade-pedestrian-bridge.
Cooperman, A., A. Eberle, and E. Lantz. 2021. "Wind turbine blade material in the United States: Quantities, costs, and end-of-life options." *Resour. Conserv. Recycl.* 168: 105439. https://doi.org/10.1016/j.resconrec.2021.105439.
Creative Pultrusion. 2022. "The new and improved pultex® pultrusion design manual of standard and custom fiber reinforced polymer structural profiles." Accessed February 15, 2022. https://f.hubspotusercontent10.net/hubfs/457166/DMV5R12%20(002).pdf.
Goodman, J. H. 2010. "Architectonic reuse of wind turbine blades." In *SOLAR 2010 ASES Conf.*, 1–8. Red Hook, NY: Curran Associates. Accessed June 18, 2021. https://www.researchgate.net/profile/Joel-Goodman-2/publication/343403060_ARCHITECTONIC_REUSE_OF_WIND_TURBINE_BLADES/links/5f28575e92851cd302d8425f/ARCHITECTONIC-REUSE-OF-WIND-TURBINE-BLADES.pdf.
Jensen, J. P., and K. Skelton. 2018. "Wind turbine blade recycling: Experiences, challenges and possibilities in a circular economy." *Renewable Sustainable Energy Rev.* 97: 165–176. https://doi.org/10.1016/j.rser.2018.08.041.
Joustra, J., B. Flipsen, and R. Balkenende. 2021a. "Structural reuse of high end composite products: A design case study on wind turbine blades." *Resour. Conserv. Recycl.* 167: 105393. https://doi.org/10.1016/j.resconrec.2020.105393.
Joustra, J., B. Flipsen, and R. Balkenende. 2021b. "Structural reuse of wind turbine blades through segmentation." *Composites, Part C: Open Access* 5: 100137. https://doi.org/10.1016/j.jcomc.2021.100137.
Liu, P., and C. Y. Barlow. 2017. "Wind turbine blade waste in 2050." *Waste Manage.* 62: 229–240. https://doi.org/10.1016/j.wasman.2017.02.007.
Luo, F., Y. Bai, and Y. Lu. 2013. "Joining pultruded FRP tubular components into space latticed shell structure–Joint design and performance." In *Proc., 4th Asia–Pacific Conf. on FRP in Structures*, 1–6. Winnipeg, MB, Canada: International Institute for FRP in Construction.
Luo, F. J., Y. Bai, X. Yang, and Y. Lu. 2016. "Bolted sleeve joints for connecting pultruded FRP tubular components." *J. Compos. Constr.* 20 (1): 04015024. https://doi.org/10.1061/(ASCE)CC.1943-5614.0000580.
Matharu, N. S., and J. T. Mottram. 2017. "Plain and threaded bearing strengths for the design of bolted connections with pultruded FRP material." *Eng. Struct.* 152: 878–887. https://doi.org/10.1016/j.engstruct.2017.10.003.
McDonald, A., C. Kiernicki, M. Bermek, Z. Zhang, A. Poff, S. Kakkad, E. Lau, F. Arias, R. Gentry, and L. Bank. 2022. "Re-wind design catalog 2nd edition fall/autumn 2022." Accessed November 9, 2022. https://static1.squarespace.com/static/5b324c409772ae52fecb6698/t/636bd07125aeb5312a8e320e/1668010099748/Re-Wind+Design+Catalog+Fall+2022+Nov+9+2022+%28low+res%29.pdf.
McMaster-Carr. 2022. "Anchor for hollow block and brick, stud-style, 3/8" diameter, 6" long – 94255A500." Accessed November 9, 2022. https://www.mcmaster.com/standard-anchors/anchor-type~toggle/.
Mishnaevsky, L., K. Branner, H. N. Petersen, J. Beauson, M. McGugan, and B. F. Sørensen. 2017. "Materials for wind turbine blades: An overview." *Materials* 10 (11): 1285. https://doi.org/10.3390/ma10111285.
Mottram, J. T., and B. Zafari. 2011. "Pin-bearing strengths for bolted connections in fibre-reinforced polymer structures." *Proc. Inst. Civ. Eng.: Struct. Build.* 164 (5): 291–305. https://doi.org/10.1680/stbu.2011.164.5.291.
Oliveux, G., L. O. Dandy, and G. A. Leeke. 2015. "Current status of recycling of fibre reinforced polymers: Review of technologies, reuse and resulting properties." *Prog. Mater. Sci.* 72: 61–99. https://doi.org/10.1016/j.pmatsci.2015.01.004.
RS Technologies Inc. 2022. "RS Pole BlindNut Technology." Accessed November 9, 2022. https://www.rspoles.com/installation-support.
Ruane, K., et al. 2022. "Material and structural characterization of a wind turbine blade for use as a bridge girder." *Transp. Res. Rec.* 2676 (8): 354–362. https://doi.org/10.1177/03611981221083619.
Satasivam, S., and Y. Bai. 2014. "Mechanical performance of bolted modular GFRP composite sandwich structures using standard and blind bolts." *Compos. Struct.* 117: 59–70. https://doi.org/10.1016/j.compstruct.2014.06.011.
Suhail, R., J.-F. Chen, T. R. Gentry, B. Tasistro-Hart, Y. Xue, and L. C. Bank. 2019. "Analysis and design of a pedestrian bridge with decommissioned FRP windblades and concrete." In *Proc., 14th Int. Symp. on Fiber-Reinforced Polymer Reinforcement of Concrete Structures*, 1–5. Belfast, UK: IIFC. Accessed August 24, 2021. www.iifc.org/wp-content/uploads/2019/09/FRPRCS14.zip.
Wu, C., Y. Bai, and J. T. Mottram. 2016. "Effect of elevated temperatures on the mechanical performance of pultruded FRP joints with a single ordinary or blind bolt." *J. Compos. Constr.* 20 (2): 04015045. https://doi.org/10.1061/(ASCE)CC.1943-5614.0000608.
Wu, C., P. Feng, and Y. Bai. 2015. "Comparative study on static and fatigue performances of pultruded GFRP joints using ordinary and blind bolts." *J. Compos. Constr.* 19 (4): 04014065. https://doi.org/10.1061/(ASCE)CC.1943-5614.0000527.